Ground-State Properties of a Polymer Chain in an Attractive Sphere

Handan Arkın*[,†,‡] and Wolfhard Janke*[,†]

[†]Institut für Theoretische Physik, Universität Leipzig, Postfach 100 920, D-04009 Leipzig, Germany
[‡]Department of Physics Engineering, Faculty of Engineering, Ankara University, Tandogan, 06100 Ankara, Turkey

ABSTRACT: We analyze the structural formation of a polymer chain inside of an attractive sphere depending on the attraction strength. Our model is composed of a coarse-grained polymer and an attractive sphere potential. Within this frame, multicanonical Monte Carlo simulations are employed to identify the global minimum energies for a polymer chain interacting with the attractive inner wall of the sphere. Different compact structures are found with varying attraction strengths, among which are spherical, three/two, or monolayer. The conformational properties of these structures are presented.
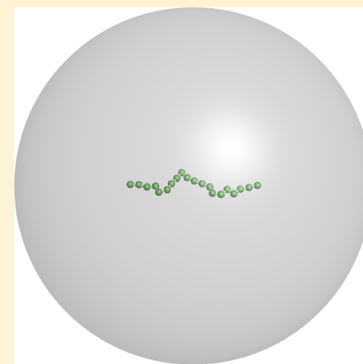
1. INTRODUCTION

Investigating basic structure formation mechanisms of biomolecules at different interfaces is one of the major challenges of a large variety of modern interdisciplinary research and possible applications in nanotechnology. Knowledge of the origin of structure formation is an important prerequisite for the understanding of polymer adhesion[1] to metals[2,3] and semiconductors,[4−6] biomedical implants,[7] and biosensors.[8] The adsorption behavior can also influence cellular motion, drug delivery, and other biological processes. The advances in designing and manipulating biomolecules at solid substrates on the nanoscale open new challenges for potential nanotechnological applications of hybrid organic−inorganic interfaces. As a result, the understanding of biomolecular structure formation near different interfaces has been recently the most intensively studied aspect from both a physical and a chemical perspective.

Recently, some progress has been achieved in this field to understand general properties of the conformational behavior of homopolymers and heteropolymers near substrates. This includes theoretical studies that, for example, have been performed to identify the structural phases and the transitions between these using scaling theory,[9,10] mean-field functional theory,[11] and numerical simulations of off-lattice models such as coarse-grained polymer chains grafted or not grafted to an attractive surface.[12−14] In most cases, the substrates are considered to be planar. The influence of curved substrates has been the subject of work only for helix formation at cylinders such as carbon nanotubes where, in all cases, the chain is outside of the curved substrate.[15−17] A qualitative deeper understanding of the basis of specific affinities is essential due to the complexity introduced by the huge amount of possible substrate structures and sequence variations for heteropolymers. Therefore, the theoretical treatment of the adsorption of macromolecules within the framework of minimalistic coarse-grained polymer models in statistical mechanics has been a longstanding problem[18,19] that still gains a lot of interest.[20−27]

In this work, we consider a simple off-lattice coarse-grained polymer model inside of an attractive sphere, for which we have recently constructed the finite-temperature phase diagram.[28] Here, we focus on the ground-state properties caused by different attraction strengths of the sphere within the frame of generalized-ensemble simulations. In a comparative analysis, a classification of the structures formed in the accompanying adsorption process has been achieved. It is one of the most remarkable results of our study that for different parameter values of the polymer-attractive sphere system, we get conformations that fit perfectly to the inner wall of the sphere. This could be a potential mechanism for designing biomedical implants and the discovery of new drugs. Further relevant applications are the development and construction of polymer coatings or the design of nanoparticles in tissue engineering. This would enable the manipulating of complex spherical nanoparticles or capsule-like particles and therefore allows for applications beyond those very well known or that are newly developed and more biocompatible.

2. MODEL

The polymer chain is described by a coarse-grained off-lattice semiflexible model for homopolymers, which has also been used for studies of heteropolymers in the frame of the hydrophobic-polar model.[29] As on the lattice, the adjacent monomers are connected by rigid covalent bonds. Thus, the distance is kept fixed and set to unity. The contact interaction of lattice models is replaced by a distance-dependent Lennard-

Jones (LJ) potential accounting for short-range excluded volume repulsion and long-range interaction. An additional interaction accounts for the bending energy of any pair of successive bonds. The position vector of the ith monomer, $i = 1, ..., N$, is denoted by $\vec{r}_i$. A polymer with N monomers has $N-1$ bonds of length unity between neighboring monomers and $N-2$ bending angles ϑ_i, defined through

$$\cos(\vartheta_i) = (\vec{r}_{i+1} - \vec{r}_i) \cdot (\vec{r}_{i+2} - \vec{r}_{i+1}) \qquad (1)$$

The LJ potential of nonbonded monomers is of standard 12−6 form. This model was first employed in two dimensions[30] and later generalized to three-dimensional AB proteins,[29,31] partially with modifications taking implicitly into account additional torsional energy contributions of each bond. The energy function for the polymer is thus given by

$$E_\mathrm{p} = 4 \sum_{i=1}^{N-2} \sum_{j=i+2}^{N} (r_{ij}^{-12} - r_{ij}^{-6}) + \frac{1}{4} \sum_{i=1}^{N-2} (1 - \cos \vartheta_i) \qquad (2)$$

In this work, we assume that the polymer chain is confined in an attractive sphere. The interaction of the polymer chain monomers with the attractive inner surface of a spherical cage is modeled as

$$E_\mathrm{s} = 4\epsilon_\mathrm{c} \frac{\pi R_\mathrm{c}}{r_i} \left\{ \frac{1}{5} \left[\left(\frac{\sigma}{R_\mathrm{c} - r_i} \right)^{10} - \left(\frac{\sigma}{R_\mathrm{c} + r_i} \right)^{10} \right] \right.$$
$$\left. - \frac{\epsilon}{2} \left[\left(\frac{\sigma}{R_\mathrm{c} - r_i} \right)^{4} - \left(\frac{\sigma}{R_\mathrm{c} + r_i} \right)^{4} \right] \right\} \qquad (3)$$

where R_c is the radius of the sphere, which is a measure of the cage size, $r_i = (x_i^2 + y_i^2 + z_i^2)^{1/2}$ is the distance of a monomer to the origin, x_i, y_i, and z_i are the coordinates of monomers, and $\sigma = 1.0$ and $\epsilon_\mathrm{c} = 1.0$. For our simulations, the polymer chain length is $N = 20$, and we set R_c large enough to enclose the polymer inside of the sphere. We also have done simulations with different sizes of the sphere ranging over $R_\mathrm{c} = 10$, 20, and 30. However, to allow the chain to circulate freely inside of the sphere and also to reduce the influence on the observables, we eventually set it to 20. The parameter ϵ in the second term of eq 3 defines the attraction strength of the sphere inner wall and weights the relative importance of intrinsic monomer−monomer and monomer−sphere wall interactions. In our simulations, ϵ is varied between 0.1 and 1.4. The total energy $E = E_\mathrm{p} + E_\mathrm{s}$ of the system is thus composed of the pure configurational polymer chain energy and the polymer chain attractive sphere interaction energy. A start configuration of the simulation is presented in Figure 1. The initial configuration of the polymer chain is randomly generated, where the ends have no contact with the sphere attractive wall. In some theoretical and computational studies, the polymer is attached ("grafted") at the surface with one of its ends, which reduces the entropic degrees-of-freedom of the system. However, in many recent experiments of, for example, peptide−metal or peptide−semiconductor interfaces, the setup of a freely moving polymer is considered. This allows for adsorbed conformations where neither of the two polymer ends is in contact with the cage.

3. METHOD

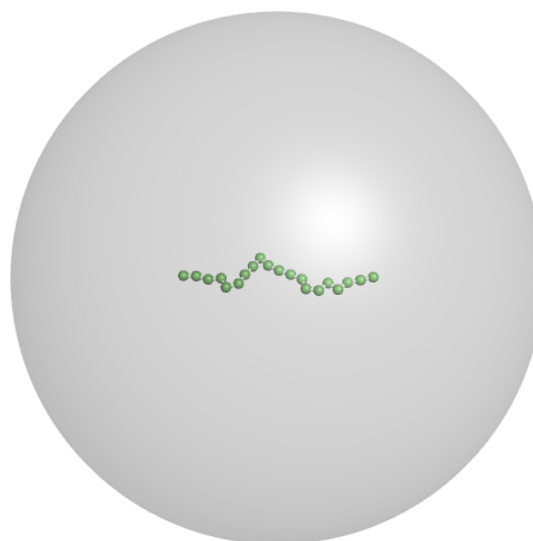In order to obtain statistical results of sufficient accuracy, we applied the multicanonical Monte Carlo algorithm[32] (for

Figure 1. The random start configuration of the simulation. For the sphere radius, we choose $R_\mathrm{c} = 20$ to let the polymer with $N = 20$ monomers circulate freely inside of the sphere.

reviews, see refs 33 and 34), where the energy distribution is flattened artificially, allowing, in principle, for a random walk of successive states in energy space. This flattening is controllable and therefore reproducible. To this end, the Boltzmann probability is multiplied by a weight factor $W(E)$, which in our case is a function of the energy. Then, the multicanonical probability for a state $\{x\}$ with energy $E(\{x\})$ reads $p_\mathrm{M}(E) = \exp(-E/k_\mathrm{B}T) W(E)$. In order to obtain a multicanonical or "flat" distribution, the initially unknown weight function $W(E)$ has to be determined iteratively. In the beginning, the weights $W^{(0)}(E)$ are set to unity for all energies, letting the first run be a usual Metropolis simulation, which yields an estimate $H^{(0)}(E)$ for the canonical distribution. This histogram is used to determine the next guess for the weights; the simplest update is to calculate $W^{(1)}(E) = W^{(0)}(E)/H^{(0)}(E)$. Then, the next run is performed with probabilities $p_\mathrm{M}^{(1)}(E) = \exp(-E/k_\mathrm{B}T) W^{(1)}(E)$ of states with energy E, yielding $H^{(1)}(E)$ and $W^{(2)}(E) = W^{(1)}(E)/H^{(1)}(E)$, and so on. The iterative procedure is continued until the weights are appropriate in a way that the multicanonical histogram $H(E)$ is flat. After having determined accurate weights $W(E)$, they are kept fixed, and following some thermalization sweeps, a long production run is performed, where statistical quantities O are obtained multicanonically, $\langle O \rangle_\mathrm{M} = \sum_{\{x\}} p_\mathrm{M}(E(\{x\})) O(\{x\})/Z_\mathrm{M}$, with the multicanonical partition function $Z_\mathrm{M} = \sum_{\{x\}} p_\mathrm{M}(E(\{x\}))$. The canonical statistics is obtained by reweighting the multicanonical to the canonical distribution, that is, mean values are computed as $\langle O \rangle = \langle OW^{-1} \rangle_\mathrm{M}/\langle W^{-1} \rangle_\mathrm{M}$.

For the determination of the multicanonical weights, we performed 200 iterations with at least 10^5 sweeps each. In the production period, 1×10^8 sweeps were generated to get a reasonable statistics and, in particular, to capture the ground states. For identification of the global minimum energies, we also employed the energy landscape paving optimization,[35] which, for this aim, performed equally well.

In order to check the structural compactness of conformations or to identify the possible dispersion of conformations because of the interaction with the sphere inner wall, the radius of gyration of the conformations is calculated. The radius of

gyration is a measure for the extension of the polymer and defined by

$$R_g^2 \equiv \frac{1}{N} \sum_{i=1}^{N} (\vec{r}_i - \vec{r}_{cm})^2 = \frac{1}{2N^2} \sum_{i=1}^{N} \sum_{j=1}^{N} (\vec{r}_i - \vec{r}_j)^2$$

$$\text{with } \vec{r}_{cm} = \frac{1}{N} \sum_{i=1}^{N} \vec{r}_i \tag{4}$$

being the center-of-mass of the polymer. We also calculated various shape descriptors derived from the gyration tensor,[36−39] which is defined as

$$S = \frac{1}{N} \begin{pmatrix} \sum_i (x_i - x_{cm})^2 & \sum_i (x_i - x_{cm})(y_i - y_{cm}) & \sum_i (x_i - x_{cm})(z_i - z_{cm}) \\ \sum_i (x_i - x_{cm})(y_i - y_{cm}) & \sum_i (y_i - y_{cm})^2 & \sum_i (y_i - y_{cm})(z_i - z_{cm}) \\ \sum_i (x_i - x_{cm})(z_i - z_{cm}) & \sum_i (y_i - y_{cm})(z_i - z_{cm}) & \sum_i (z_i - z_{cm})^2 \end{pmatrix} \tag{5}$$

Transformation to the principal axis system diagonalizes S

$$S = \text{diag}(\lambda_1, \lambda_2, \lambda_3) \tag{6}$$

where we assume that the eigenvalues of S are sorted in descending order, that is, $\lambda_1 \geq \lambda_2 \geq \lambda_3$. The first invariant of S gives the squared radius of gyration

$$\text{Tr } S = \lambda_1 + \lambda_2 + \lambda_3 = R_g^2 \tag{7}$$

which agrees with the definition given in eq 4. The second invariant shape descriptor, or relative shape anisotropy, is defined as

$$\kappa^2 \equiv A_3 = \frac{3}{2} \frac{\text{Tr } \hat{S}^2}{(\text{Tr } S)^2} = 1 - 3 \frac{\lambda_1\lambda_2 + \lambda_2\lambda_3 + \lambda_3\lambda_1}{(\lambda_1 + \lambda_2 + \lambda_3)^2} \tag{8}$$

where $\hat{S} = S - 1/3(\text{Tr } S)E$, with unit tensor E. It reflects both the symmetry and dimensionality of a polymer conformation. This parameter is limited between the values of 0 and 1. It reaches 1 for an ideal linear chain and drops to 0 for highly symmetric conformations. For planar symmetric objects, the relative shape anisotropy converges to the value of 1/4.[36,37,39,40] The last descriptor, the asphericity parameter b, measures the deviation from the spherical symmetry (recall that λ_1 is the largest eigenvalue)

$$b = \lambda_1 - \frac{1}{2}(\lambda_2 + \lambda_3) \tag{9}$$

Another useful quantity is the mean number of monomers docked to the surface. A single-layer structure is formed if all monomers are attached at the sphere; if none are attached, the polymer is desorbed. The sphere potential is a continuous potential, and in order to distinguish monomers docked to the sphere inner wall from those not being docked, it is necessary to introduce a cutoff. We define a monomer i as being "docked" if $R_c - r_i < r_c \equiv 1.2$. The corresponding measured quantity is the average number $\langle N_s \rangle$ of monomers docked to the inner wall. Formally, this can be expressed as

$$N_s = \sum_{i=1}^{N} \theta(r_c - r_i) \tag{10}$$

where $\theta(r)$ is the Heaviside step function.

4. RESULTS AND DISCUSSION

First, we show the distributions of all successive pairs of virtual bond angles $\Theta_i = \pi - \vartheta_i$ and torsion angles Φ_i for the homopolymer in the low-temperature regime ($T < 0.2$) for different values of the attraction strength ϵ in Figure 2. These
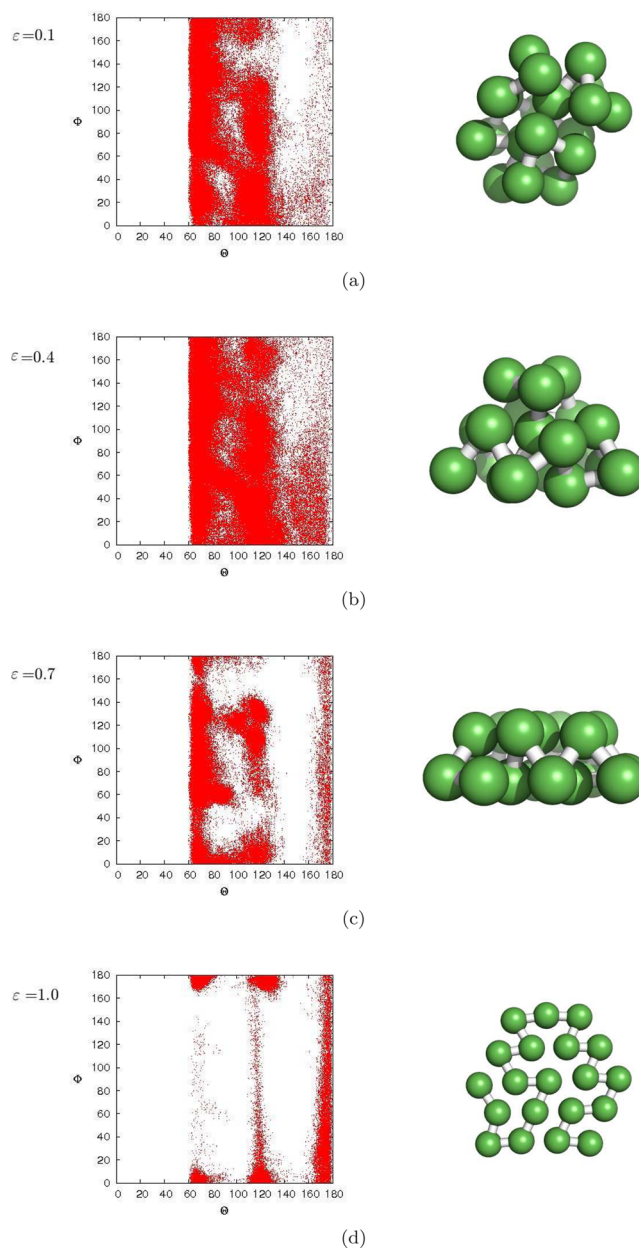

Figure 2. Bond and torsion angle distributions for ϵ = (a) 0.1, (b) 0.4, (c) 0.7, (d) 1.0, and the associated global minimum-energy conformations. The distribution of the torsion angles has reflection symmetry, and therefore, only the positive interval is shown. There are no differences with other intervals.

plots are analogous to the Ramachandran plots for proteins, which give the distribution of dihedral angles and signal secondary structure for the proteins. With the angle distributions, the ground-state conformations are also depicted. The first plot for $\epsilon = 0.1$ corresponds to the most compact conformation that is minimally affected by the attractive sphere. This is an almost spherically symmetric compact structure inside of the sphere. As expected, the virtual bond and torsion
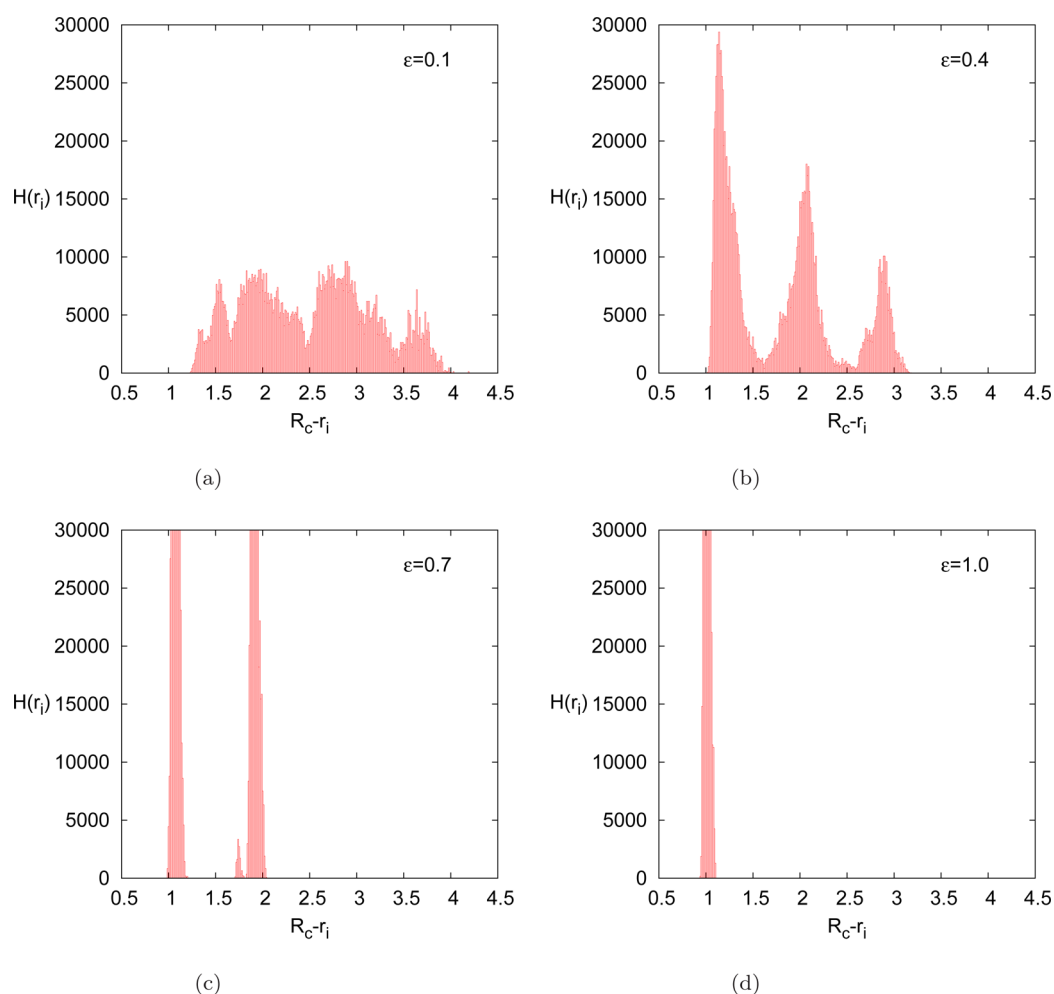
Figure 3. Radial distributions of monomers of minimum-energy conformations for ϵ = (a) 0.1, (b) 0.4, (c) 0.7, and (d) 1.0.

angles distribution is a randomly scattered plot. Because the polymer chain has no position constraint, it circulates freely within the whole space inside of the sphere (recall that it is not grafted by one of its ends). Nevertheless, we observe two domains dominant in the distribution for bond angles from 60 to 80° and segments with bond angles between 100 and 130° for a broad distribution of torsion angles. The angles are close to 60, 90, and 120° as these angles are typical base angles in face-centered cubic crystals. However, this concerns only segments of the conformations as these distributions are accumulated distributions of the degrees of freedom. The second plot for ϵ = 0.4 belongs to the region where partially adsorbed, compact three-layer conformations are found as global minimum-energy states. The lowest layer of the conformations is adsorbed and lies on the inner wall of the sphere. The other layers stay on top of it to build a pyramide-like shape. These are the most similar conformations to the first case of very weak attraction (spherically symmetric structures). Therefore, the angle distribution looks similar to that for ϵ = 0.1. The only difference here is the newly developing branch in the higher bond angles (160−180°), which belongs to the almost straight segments that occur in the lowest layer. By further increasing the attraction strength to ϵ = 0.7, deviations in the angle distribution come out, and the global minimum-energy conformations also change significantly. These are now partially adsorbed two-layer conformations. The scatter plot is now confined to some regions, and the other parts are not

allowed by the conformations. For ϵ = 1.0, we have single-layer conformations as the global minimum states. These single-layer structures lie on the inner wall of the sphere and fit the sphere wall perfectly, and the virtual bond and torsion angles allowed by the conformations are confined in small regions. The reason can be seen from the three-dimensional plot of the global minimum state for ϵ = 1.0. The virtual bond angles are confined to three regions between 60−80, 110−130, and 170−180°.

For a detailed illustration, we plot in Figure 3 the radial distribution of monomers with respect to the distance from the sphere $R_c - r_i$ of low-energy conformations, that is, the conformations that have energies less than one unit above the ground-state energy of the system under consideration with varying attraction strength. One can conclude that accumulations of monomers are seen at different distances from the sphere, that is, different layers are obviously seen in the respective structures in Figure 2. In Figure 3a, the radial distributions of monomers for low attraction strength of the sphere are shown. The structure is spherically symmetric, and the radial distribution of monomers reflects this property. A clear three-layer structure can be identified in Figure 3b, where the ground-state conformation in this phase is shown in Figure 2b. Further increasing the attraction strength of the sphere causes a radial distribution of monomers in a clear two-layer structure (Figure 3c), which transforms into a monolayer at $\epsilon \geq$ 1.0, as depicted in Figure 3d.
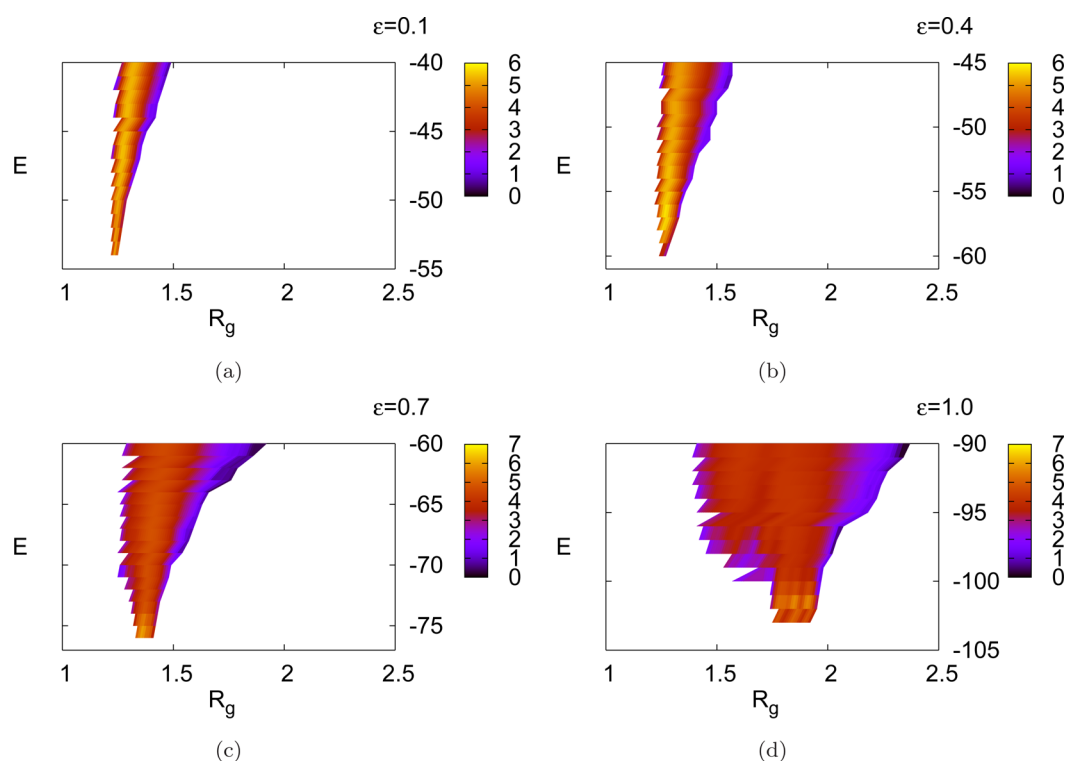
Figure 4. Radius of gyration R_g distributions in the low-energy regime for ϵ = (a) 0.1, (b) 0.4, (c) 0.7, and (d) 1.0.
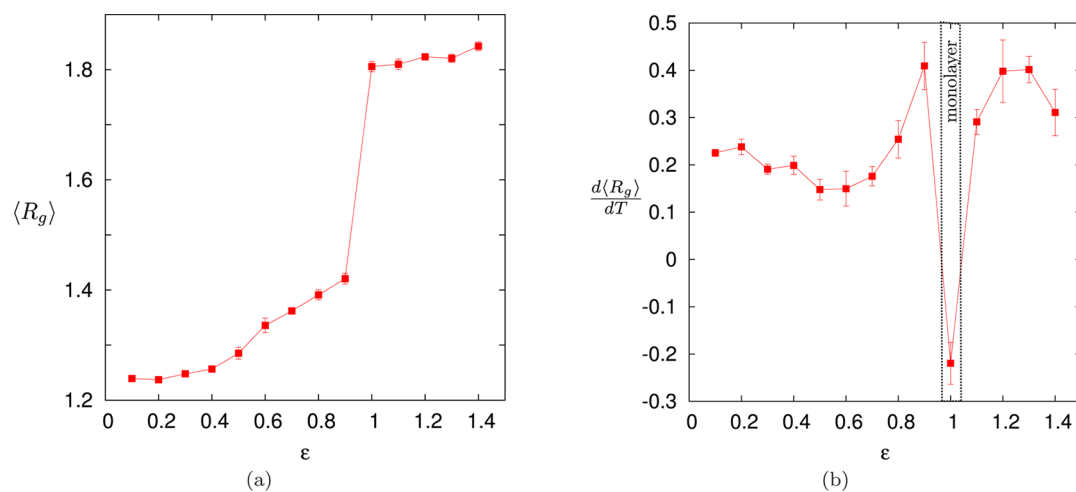

Figure 5. (a) The radius of gyration $\langle R_g \rangle$ and (b) its temperature derivative as a function of the attraction strength ϵ of the sphere.

The radius of gyration shows an excellent view whether the conformations are compact or not; more precisely, we can also get a sense into the layering structure of conformations for very high sphere attraction strengths. Figure 4 presents the multicanonical histograms $H(E,R_g)$ for different ϵ values. These figures cover a little wider range of energies than Figures 2 and 3 for a better overview. For ϵ = 0.1, only the phase with globular structures is visible, and at low temperature, there is only one sharp R_g value, which corresponds to the spherically shaped compact ground-state structures. The increase of ϵ leads to some minimal change at ϵ = 0.4. Because at this ϵ value the ground-state structures are three-layer structures that are also still close to spherical shape, as said before, this crossover can be better distinguished by the $\langle N_s \rangle$ parameter of adsorbed monomers. However, note that the minimum energies are also shifted to much lower energies. This

clearly indicates that the polymer sticks to the wall of the sphere. At ϵ = 0.7, the space broadens while the energies E_p and E_s compete. Additionally, the low-energy part is shifted to higher R_g values. Further increasing ϵ to ϵ = 1.0 causes more broadening in the conformational space and also more shifting in the R_g values.

In Figure 5a and b, the mean radius of gyration $\langle R_g \rangle$ and its temperature derivative $d\langle R_g \rangle/dT$ are given at temperature T = 0.2 as a function of the attraction strength ϵ of the sphere, respectively. For small values of ϵ, ϵ = 0.1, 0.2, 0.3, and 0.4, the most compact conformations occur in the low-temperature region with an average $\langle R_g \rangle \approx 1.23$. Further increasing the ϵ value causes also an increase in the average $\langle R_g \rangle$ value to about 1.4. Increasing the ϵ parameter further, $\langle R_g \rangle$ jumps to 1.8 at ϵ = 1.0. Above ϵ = 1.0, all other ϵ values have the typical value $\langle R_g \rangle$ = 1.8. This jump is also detectable from its temperature
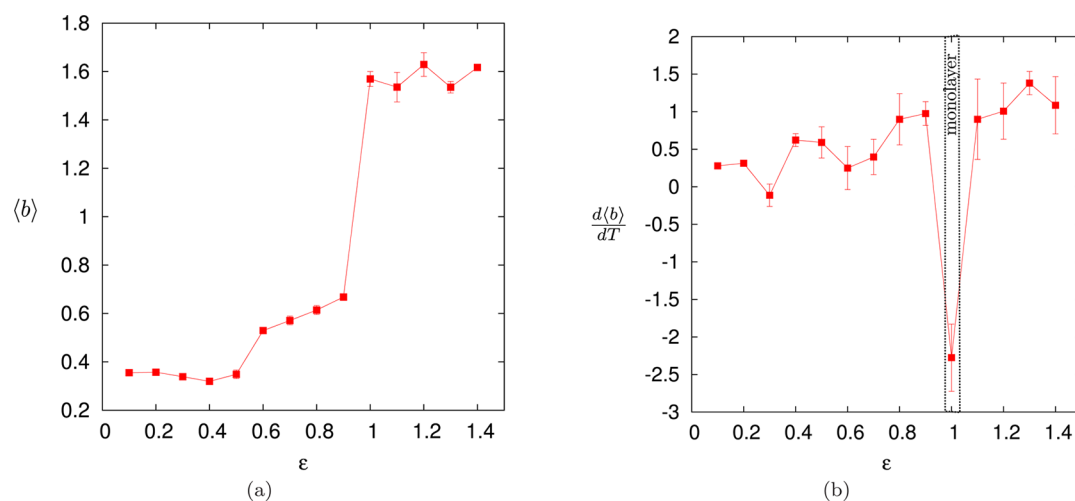
Figure 6. (a) The asphericity parameter $\langle b \rangle$ and (b) its temperature derivative as a function of the attraction strength ϵ of the sphere.
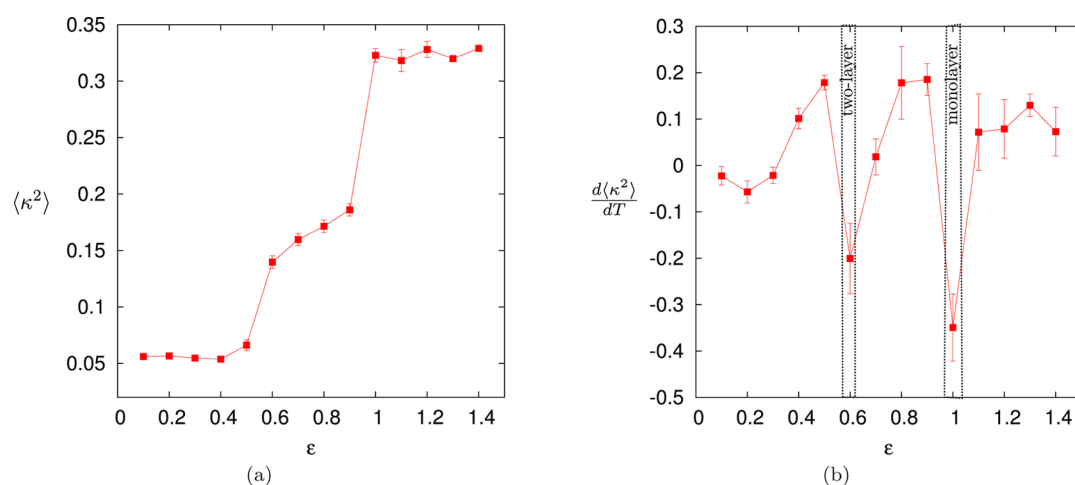

Figure 7. (a) The relative shape anisotropy parameter $\langle \kappa^2 \rangle$ and (b) its temperature derivative as a function of the attraction strength ϵ of the sphere.

derivative shown in Figure 5b, which has a negative sign at $\epsilon = 1.0$. As a function of temperature, the radius of gyration is monotonically increasing for all ϵ values except at $\epsilon = 1.0$,[28] where the layering transition occurs. At this value, the radius of gyration has a minimum at $T = 0.37$. Hence, the temperature derivative has a negative sign at $T = 0.2$. In other words, for $\epsilon = 1.0$, the tangential line to the curve at $T = 0.2$ has an obtuse angle, while the others have an acute angle. From our recently constructed finite-temperature phase diagram in the $\epsilon - T$ plane,[28] it can be seen why this is so. For very low temperatures, one passes at $\epsilon = 1.0$ with increasing temperature the phase transition from the extended monolayer with a relatively large radius of gyration to two-layer conformations having a smaller radius of gyration.

From there on, we can conclude that the most pronounced transition is the layering transition that occurs at $\epsilon = 1.0$ and separates the conformational spaces of planar conformations that are one-layer conformations that are totally adsorbed to the sphere inner wall. Because the asphericity parameter b is also a linear combination of the eigenvalues of the gyration tensor, the same typical jump occurs also in the mean value of the asphericity parameter $\langle b \rangle$ and in its temperature derivative at $\epsilon = 1.0$ (Figure 6a and b). For small values of ϵ, the asphericity parameter is smaller because the conformations are almost spherically symmetric, but for larger ϵ values, it starts to

deviate, and at $\epsilon = 1.0$, it jumps significantly. The temperature derivative of the asphericity parameter also has a negative sign at $\epsilon = 1.0$ for the same reason as mentioned for the radius of gyration. More details of the shape characteristics are revealed by the relative shape anisotropy, which is shown in Figure 7. In our simulations, the compact, spherically shaped conformations reach an average value of $\langle \kappa^2 \rangle \approx 0.05$ for a smaller attraction strength ($\epsilon = 0.1, 0.2, 0.3,$ and 0.4). It should be noted that due to the covalent bonds between adjacent monomers, even in the low-temperature regime, fluctuations occur, and the polymer low-energy states are highly degenerate, which we know are elongated from the perfect spherical shape. A precise determination of the degeneracy of states is not straightforward in our case because importance sampling methods do not enable this without extra effort. In lattice models, on the other hand, usually simple sampling algorithms are employed[22−24] that have the advantage of allowing the estimation of the degeneracy of states absolutely. Increasing the attraction strength causes also an increase in this parameter, signaling that the conformations are not spherically symmetric anymore. Rather, two-layer structures dominate in this regime ($\langle \kappa^2 \rangle \approx 0.16$). Further increasing ϵ, we detect at $\epsilon = 1.0$ the layering transition where $\langle \kappa^2 \rangle$ reaches approximately a value of 0.32. This is a topological transition from 3D to 2D polymer conformations. Moreover, contrary to $\langle R_g \rangle$ and $\langle b \rangle$, $\langle \kappa^2 \rangle$ also
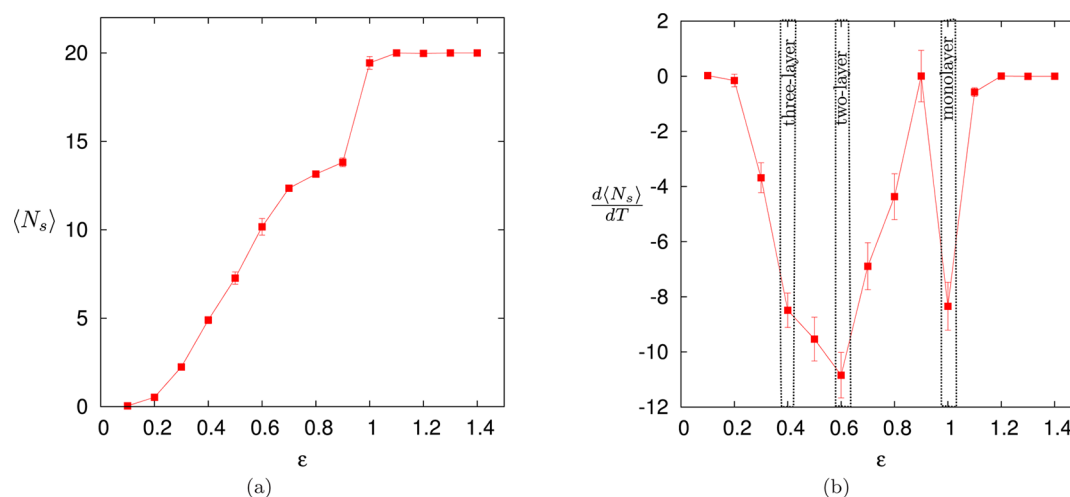
Figure 8. (a) The mean number of surface contacts $\langle N_s \rangle$ and (b) its temperature derivative as a function of the attraction strength ϵ of the sphere.

signals other transitions than the monolayer transition. In fact, one clearly identifies the transition that separates the two-layer and three-layer pseudophases at $\epsilon = 0.6$ by looking at the temperature derivative of the relative shape anisotropy parameter in Figure 7b. The relative shape anisotropy parameter has two minima in the temperature dependence, one at $\epsilon = 0.6$ and one at $\epsilon = 1.0$, where the tangential lines give obtuse angles signaled by the negative sign of its temperature derivative at these transition points.

Further important results are illustrated in Figure 8a and b, where we plot the mean number of monomers docked to the inner surface of the sphere and its temperature derivative at temperature $T = 0.2$ as a function of the attraction strength of the sphere. Because the adsorption phenomena typically affect only segments of the polymer, calculating this parameter is the best way for discussing the adsorption process. Above $\epsilon = 1.0$, all of the monomers are adsorbed to the inner wall of the sphere where $\langle N_s \rangle$ equals the chain length $N = 20$. Below $\epsilon = 1.0$, decreasing the ϵ value leads to decreasing $\langle N_s \rangle$ values, which vanish at $\epsilon = 0.1$. That means that at this value, the chain is completely desorbed and moves freely inside of the sphere without a noticeable influence of the attractive sphere. For a detailed discussion, we finally concentrate on the temperature fluctuations of the mean number of monomers docked to the inner wall of the sphere, $d\langle N_s \rangle/dT$, displayed in Figure 8b. Because the mean number of adsorbed monomers is largest at low temperatures and decreases with increasing temperature, the temperature derivative of this parameter is negative at all points. We observe two peaks and one shoulder corresponding to the three-layer ($\epsilon \approx 0.4-0.5$), two-layer ($\epsilon \approx 0.6$), and monolayer ($\epsilon \approx 1.0$) transitions, respectively, where we determine these points also with the other structural observables. Because of the larger number of degrees of freedom for the off-lattice polymer, higher-order layering transitions cannot be identified in our analyses.

Finally, in order to compare our results with those for a polymer adsorbing to a plane surface obtained previously by Möddel et al.,[12] we related our attraction strength ϵ with the attraction strength ϵ_s of the flat surface model by comparing the minima of the 9−3 LJ potential used in ref 12 and our 10−4 LJ-like potential (eq 3). Although the two potentials have some functional differences, we obtained quite a good agreement of the low-temperature transition points by using this mapping.[41]

5. CONCLUSION

In this paper, we have studied the structure formation of a coarse-grained off-lattice polymer model inside of an attractive sphere. The main goal of the study was to identify the different morphologies of polymer ground-state conformations, depending on the attraction strength of the sphere inner wall. We found that at low attraction strength, the conformations are spherically symmetric compact structures, which is also the main property of a freely moving polymer without being in interaction with its environment. As we know from previous studies of the high-temperature regime, a collapse transition from extended random coils to a more compact, globular phase occurs, which is rather weak, such that this transition can hardly be identified in the specific-heat curves. Much more pronounced is the low-temperature transition that signals further structural compacting. The mean values of structural parameters such as the radius of gyration (R_g), the asphericity (b), and the relative shape anisotropy (κ^2) show that, on average, the structures reach a spherical compact shape. However, even in the low-temperature regime, fluctuations occur, and the polymer low-energy states are highly degenerate, which we know are elongated from the perfect spherical shape. The presence of an attractive sphere strongly affects the ground-state property of the polymer at the interface for stronger interactions. The monomer−monomer and the monomer−sphere interactions compete with each other, and this competition results in different ground states depending on the attraction strength. Moreover, we found detectable jumps in the mean values of structural parameters such as κ^2 and the number of surface contacts (N_s), indicating these layering transitions. Increasing the attraction strength causes three-layer and two-layer structures whose first layer is adsorbed to the sphere inner wall. For sufficiently high attraction strengths, we observe the formation of single-layer structures that perfectly fit the spherical confinement. These observations could enable a wide variety of potential applications in a controlled way, ranging from biocompatible medical implant modification to polymer coating.

AUTHOR INFORMATION

Corresponding Author
*E-mail: Handan.Arkin@itp.uni-leipzig.de (H.A.); Wolfhard. Janke@itp.uni-leipzig.de (W.J.). Homepage: http://www. physik.uni-leipzig.de/CQT.html.

Notes
The authors declare no competing financial interest.

ACKNOWLEDGMENTS

REFERENCES

(1) Walheim, S.; Schaffer, E.; Mlynek, J.; Steiner, U. *Science* **1999**, *283*, 520.
(2) Brown, S. *Nat. Biotechnol.* **1997**, *15*, 269.
(3) Braun, R.; Sarikaya, M.; Schulten, K. *J. Biomater. Sci., Polym. Ed.* **2002**, *13*, 747.
(4) Whaley, S. R.; English, D. S.; Hu, E. L.; Barbara, P. F.; Belcher, A. M. *Nature* **2000**, *405*, 665.
(5) Goede, K.; Busch, P.; Grundmann, M. *Nano Lett.* **2004**, *4*, 2115.
(6) Bachmann, M.; Goede, K.; Beck-Sickinger, A. G.; Grundmann, M.; Irbäck, A.; Janke, W. *Angew. Chem., Int. Ed.* **2010**, *49*, 9530.
(7) Nakata, E.; Nagase, T.; Shinkai, S.; Hamachi, I. *J. Am. Chem. Soc.* **2004**, *126*, 490.
(8) Service, R. F. *Science* **1995**, *270*, 230.
(9) Eisenriegler, E.; Kremer, K.; Binder, K. *J. Chem. Phys.* **1982**, *77*, 6296.
(10) Usatenko, Z. *J. Stat. Mech.* **2006**, P03009.
(11) Forsman, J.; Woodward, C. E. *Phys. Rev. Lett.* **2005**, *94*, 118301.
(12) Möddel, M.; Bachmann, M.; Janke, W. *J. Phys. Chem. B* **2009**, *113*, 3314.
(13) Möddel, M.; Janke, W.; Bachmann, M. *Phys. Chem. Chem. Phys.* **2010**, *12*, 11548.
(14) Möddel, M.; Janke, W.; Bachmann, M. *Macromolecules* **2011**, *44*, 9013.
(15) Milchev, A.; Binder, K. *J. Chem. Phys.* **2002**, *117*, 6852.
(16) (a) Gurevitch, I.; Srebnik, S. *Chem. Phys. Lett.* **2007**, *444*, 96. (b) Gurevitch, I.; Srebnik, S. *J. Chem. Phys.* **2008**, *128*, 144901.
(17) Vogel, T.; Bachmann, M. *Phys. Rev. Lett.* **2010**, *104*, 198302.
(18) Eisenriegler, E., *Polymers near Surfaces*; World Scientific: Singapore, 1993.
(19) Fleer, G. J.; Cohen Stuart, M. A.; Scheutjens, J. M. H. M.; Cosgrove, T.; Vincent, B. *Polymers at Interfaces*; Chapman and Hall: London, 1993.
(20) Diehl, H. W.; Shpot, M. *Nucl. Phys. B* **1998**, *528*, 595.
(21) Sikorski, A. *Macromol. Theory Simul.* **2002**, *11*, 359.
(22) Bachmann, M.; Janke, W. *Phys. Rev. Lett.* **2005**, *95*, 058102.
(23) Bachmann, M.; Janke, W. *Phys. Rev. E* **2006**, *73*, 041802.
(24) Bachmann, M.; Janke, W. *Phys. Rev. E* **2006**, *73*, 020901(R).
(25) Binder, K.; Baschnagel, J.; Müller, M.; Paul, W.; Rampf, F. *Macromol. Symp.* **2006**, *237*, 128.
(26) Luettmer-Strathmann, J.; Rampf, F.; Paul, W.; Binder, K. *J. Chem. Phys.* **2008**, *128*, 064903.
(27) Karalus, S.; Janke, W.; Bachmann, M. *Phys. Rev. E* **2011**, *84*, 031803.
(28) Arkin, H.; Janke, W. *Phys. Rev. E* **2012**, *85*, 051802.
(29) Irbäck, A.; Peterson, C.; Potthast, F.; Sommelius, O. *J. Chem. Phys.* **1997**, *107*, 273.
(30) (a) Stillinger, F. H.; Head-Gordon, T.; Hirshfeld, C. L. *Phys. Rev. E* **1993**, *48*, 1469. (b) Stillinger, F. H.; Head-Gordon, T. *Phys. Rev. E* **1995**, *52*, 2872.
(31) Irbäck, A.; Peterson, C.; Potthast, F. *Phys. Rev. E* **1997**, *55*, 860.
(32) (a) Berg, B. A.; Neuhaus, T. *Phys. Lett. B* **1991**, *267*, 249. (b) Berg, B. A.; Neuhaus, T. *Phys. Rev. Lett.* **1992**, *68*, 9. (c) Berg, B. A.; Çelik, T. *Phys. Rev. Lett.* **1992**, *69*, 2292. (d) Janke, W. *Int. J. Mod. Phys. C* **1992**, *3*, 1137.
(33) Berg, B. A. *Fields Institute Communications* **2000**, *26*, 1.
(34) Janke, W. *Physica A* **1998**, *254*, 164.
(35) (a) Hansmann, U. H. E.; Wille, L. T. *Phys. Rev. Lett.* **2002**, *88*, 068105. (b) Arkın, H.; Çelik, T. *Eur. Phys. J. B* **2002**, *30*, 577.
(36) Solc, K.; Stockmayer, W. H. *J. Chem. Phys.* **1971**, *54*, 2756.
(37) Theodorou, D. N.; Suter, U. W. *Macromolecules* **1985**, *18*, 1206.
(38) Blavatska, V.; Janke, W. *J. Chem. Phys.* **2010**, *133*, 184903.
(39) Vymětal, J.; Vondrášek, J. *J. Phys. Chem. A* **2011**, *115*, 11455.
(40) Blavatska, V.; Janke, W. *J. Chem. Phys.* **2012**, *136*, 104907.
(41) Arkın, H.; Janke, W. Leipzig preprint. *Eur. Phys. J.* Special Topics; **2012** In press.